Journal of Molecular Graphics and Modelling 37 (2012) 67–76

Contents lists available at SciVerse ScienceDirect

Journal of Molecular Graphics and Modelling

journal homepage: www.elsevier.com/locate/JMGM

QM/MM study of catalytic mechanism of Xylanase Cex from *Cellulomonas fimi*

Jingli Liu [a], Chunchun Zhang [b], Dingguo Xu [a,*]

[a] MOE Key Laboratory of Green Chemistry and Technology, College of Chemistry, Sichuan University, Chengdu, Sichuan 610064, China
[b] Analytical & Test Center, Sichuan University, Chengdu, Sichuan 610064, China

ARTICLE INFO

Article history:
Received 16 February 2012
Received in revised form 1 April 2012
Accepted 17 April 2012
Available online 24 April 2012

Keywords:
QM/MM
Molecular dynamics
Xylanase
Substrate distortion
Retention mechanism

ABSTRACT

Xylanase Cex from *Cellulomonas fimi* is a bifunctional enzyme that catalyzes the degradation of both cellulose and xylan. As a result, it might find valuable applications in production of biofuels. In this work, we presented a detailed theoretical investigation of hydrolysis of the xylopentaose molecule catalyzed by Cex, using a hybrid quantum mechanical and molecular mechanical approach. Our results support the experimental observation that the hydrolysis proceeds via the net retention mechanism. More interestingly, our simulations indicate that the xylose unit at −1 binding site should take a boat ($B_{2,5}$) conformation as a possible reactive conformer, while the oxo-carbenium ion-like transition states take the combination of $B_{2,5}/{}^{O}S_2$ for glycosylation, and ${}^{O}S_2/{}^{0,3}B$ for deglycosylation. Our molecular dynamics simulations of mutants further suggest that two catalytic residues (E127 and E233) play the vital role in this ring distortion. Indeed, this conformational change is necessary to facilitate the first step of nucleophilic attack by E233 at the anomeric carbon center.

1. Introduction

As fossil fuels dwindle, the energy problem becomes one of the most challenging issues in our society. Therefore, it is highly desired to explore alternative energy sources [1–3]. Biomass based energy sources are both environmentally friendly and economically viable, thus holding a promising future. Cellulose and xylan are the most abundant components in biomass based materials, like the plant tissues. For this reason, the biodegradation of cellulose and xylan has received extensive interests [2,3].

The backbone of xylan is connected by β-1,4-linked xylopyranose units and has side chains that often consist of other sugar residues, such as arabinose and glucuronic acid [4,5]. Xylanases belong to the glycoside hydrolase (GH) superfamily, which contains over 100 family members. GH is believed to be one of the most efficient catalysts that catalyze the cleavage of the β-1,4-glycosidic bond. The detailed information about this subfamily or protein sequence can be found at the website (http://www.cazy.org/fam/acc_GH.html) [6]. In 1950, the general mechanisms for glycoside hydrolases were summarized by Koshland [7] and detailed descriptions of the catalytic mechanism for GH enzymes are given in several excellent reviews [8–11]. As depicted in Scheme 1, two different stereochemical reaction mechanisms for the GH superfamily enzymes by different stereospecific pathways, namely retention and inversion, are possible. Clearly, for the retention mechanism, the reaction takes a double displacement process via a stable covalent glycosyl-enzyme intermediate, whereas for inverting pathway, the reaction consists of a single nucleophilic substitution with only one transition state. Despite different intrinsic stereochemical characteristics for two mechanisms, some common features can be found for two pathways, e.g., an oxocarbenium ion-like transition state should be present and two conserved carboxylate group containing residues (either Glu or Asp) should exist in the active site.

Xylanases are found in the 5, 7, 8, 10, 11, and 43 subfamilies of the GH superfamily [4]. The enzymes in subfamilies 5, 7, 10 and 11 are found to take the typical retention mechanism, while enzymes in subfamilies 8 and 43 typically catalyze the hydrolysis of xylan via inversion of the anomeric center and a glutamate and aspartate are believed to be the catalytic residues. Most of reported xylanases can be grouped into family 10 and 11 [12]. Due to their roles in the food and paper industries [13], there are extensive mutagenesis and structural studies on these two families. Crystal structures for xylanases have been resolved from both bacteria [14–17] and fungi [18,19]. The topological structures of family 10 xylanases fold into a $(\alpha/\beta)_8$-barrel with a deep active site crevice [20,21], whereas xylanases in family 11 have β-jelly roll features [22].

In most cases, xylanases are glycoside hydrolases with specific activities towards bio-degradation of xylan. However, some xylanases also exhibit activities towards cellulose. An example of such bifunctional hydrolases is the β-1,4-glycannase/xylanase Cex from *Cellulomonas fimi* [23,24]. Thanks to its extensive applications in the paper and animal food industries, its mechanism and thermostability have received much attention [5,24–29]. Cex

* Corresponding author.
E-mail address: dgxu@scu.edu.cn (D. Xu).

1093-3263/$ – see front matter © 2012 Elsevier Inc. All rights reserved.
http://dx.doi.org/10.1016/j.jmgm.2012.04.005

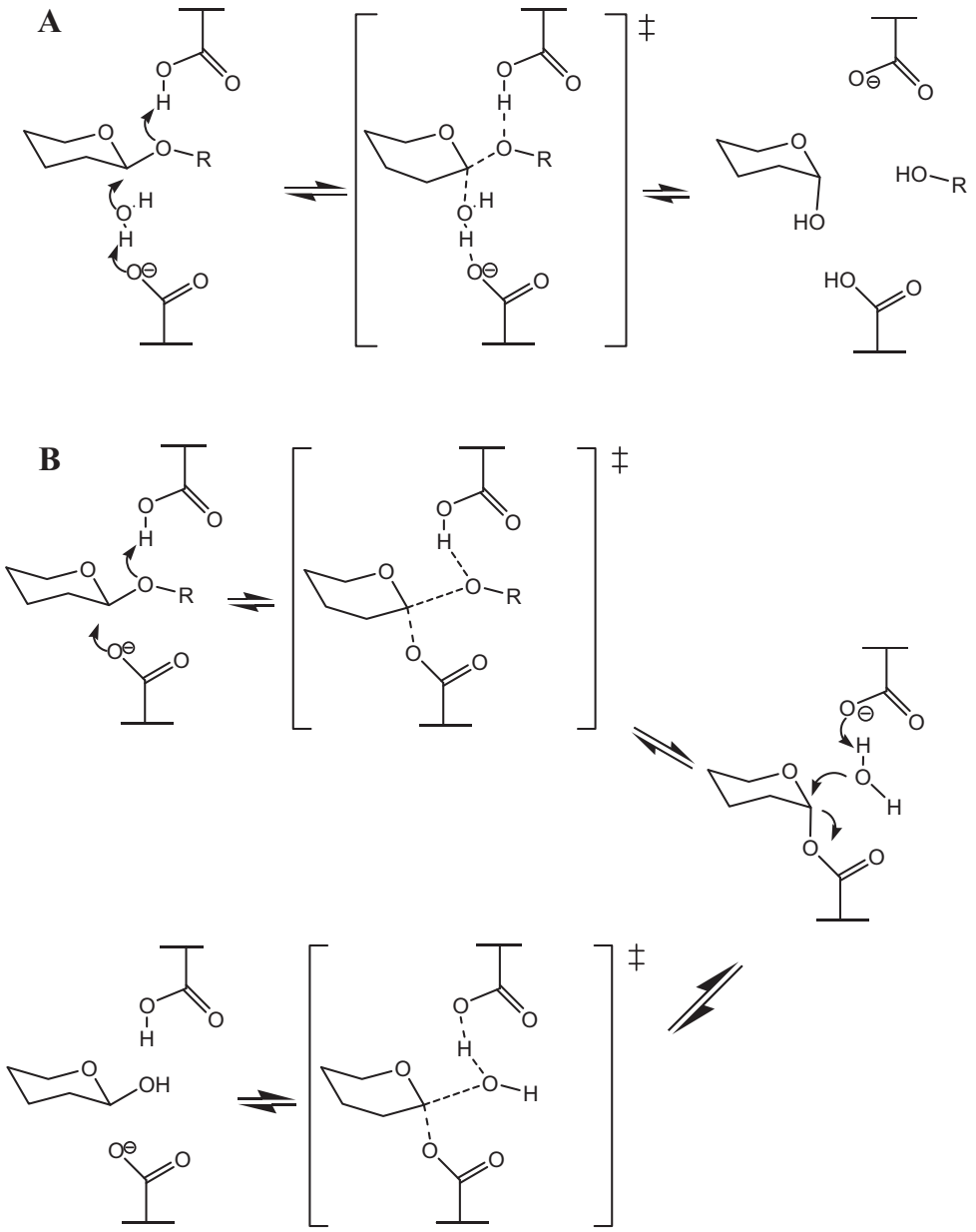

Scheme 1. General inverting (A) and retaining (B) mechanisms for the hydrolysis of β-1,4-glycosydic bond.

was first classified as a cellulase. However, it was later identified as an xylanase because its catalytic efficiency (k_{cat}/K_m) for hydrolyzing aryl xylobiosides is 30–100 times higher than those for the corresponding aryl cellobiosides [30]. This is important in paper and animal food manufacture industries, because the degradation specificity to xylan is preferred. On the other hand, the bifunctionality of Cex can be leveraged in the biofuel industry. Indeed, applications of xylanase in the conversion of biomass to fermentable sugars have been reported [31]. A detailed understanding of the catalytic mechanism of this enzyme will be helpful for further protein engineering study to enhance its bioenergy conversion efficiency.

The Cex enzyme from *C. fimi* is identified as the XynA and belongs to the GH10 subfamily. Similar with other members in the GH10 subfamily, Cex has a deep crevice on the surface that can accommodate as long as five xylose units with three glycone and two aglycone binding sites [32]. Two glutamate residues, Glu127 and Glu233, were unambiguously identified to be important for the hydrolysis of carbohydrates [14]. A recent crystallographic structure of glycosyl-enzyme intermediate strongly supports the hypothesis that the hydrolysis catalyzed by this enzyme should be via a double displacement mechanism [33]. More importantly, two thio-substituted substrate molecules have been crystallized in the active site of Cex [34], in which the thio-xylotetraose occupies the −3, −2, −1 and +1 subsites (PDB code 3CUI), while the thio-xylopentaose occupies the −3, −2, −1, +1 and +2 subsites (PDB code 3CUJ). In this work, we adapt the nomenclature of sugar units following the definition by Davies et al. [35]. The enzyme cleaves the glycosyl bond between +1 and −1 subsites. Particularly, the prefix symbol of + represents the reducing group, while the symbol of − represents the non-reducing group. Meanwhile, experimental kinetic analysis and mutagenesis studies clearly indicated that Glu127 serves as the general acid/base, while Glu233 as the nucleophile [25].

In addition to the experimental efforts to understand the mechanism, theoretical studies have been carried out to investigate the

conformational distortion in substrate binding and catalytic mechanism for xylanases. In a recent classical molecular dynamics (MD) simulation of the substrate binding of Cex, a twisted boat conformation at −1 site was suggested as a possible reactive conformer [36]. Williams and coworkers studied the substrate distortion and hydrolysis mechanism of the endo-β-1,4-xylanase from *B. circulans* (BCX) using an AM1/OPLS MD approach [37,38]. Indeed, distortion at −1 binding site seems to be a common character for glycoside hydrolases [39–42]. However, there is no consensus that what effects can cause this distortion. In this work, we will try to understand the sugar ring distortion and the detailed catalytic processes by Cex from *C. fimi* using a hybrid quantum mechanical and molecular mechanical (QM/MM) method [43].

2. Computational methods

QM/MM models. QM/MM method [43] has been widely used to study extended systems, including enzymes. The principles and applications of QM/MM approach have been discussed extensively in the literature [44–47]. Here, only a brief description is given. In the QM/MM approach, the whole system is divided into two regions: the smaller reactive region is treated with a quantum mechanical (QM) method, while the rest of system is described by a molecular mechanical (MM) approach. Therefore the QM/MM method has the advantage of accuracy of the QM method, and efficiency of the MM method.

In this work, the self-consistent charge-density functional tight binding (SCC-DFTB) method [48] was selected for the electronic structure calculation of QM region, which has been integrated into CHARMM suite of programs [49]. Its computational efficiency is comparable to other semi-empirical methods like AM1 or PM3. The hybrid SCC-DFTB/MM approach has been extensively applied to simulate various enzymatic systems, including many zinc containing enzymes [50–52]. Recently, we have studied one of prototypical retaining glycosidases, Cel5A from *Acidothermus cellulolyticus*, using this method [53]. The atoms in the MM region were described using the CHARMM22 all atom force filed [54].

The initial structure was extracted from the Protein Data Bank (PDB code 3CUJ) [34], which is an X-ray structure of Cex from *C. fimi* complexed with a thio-substituted β-1,4-xylopentaose molecule. Such a complex structure provides a good starting point for simulations of substrate binding and catalysis. The sulfur atoms were replaced with oxygen atoms to recover the true substrate molecule, xylopentaose, and corresponding initial guess of the enzyme–substrate (ES) complex. The atom definition and interactions between the substrate and active site residues are given in Scheme 2. As the acid/base catalyst, E127 is modeled in its neutral form, while E233 in the ionized form. H205 was simulated with a positive charged side chain due to hydrogen bonds with E233 and D235. In addition, the disulfur bonds between C167 and C199, C261 and C267 were enforced.

The ES complex was solvated using a pre-equilibrated TIP3P [55] water sphere with a 25 Å radius centered at the C_1 (−1) atom. This process was repeated several times with rotated water spheres to ensure uniform solvation. The solvent was relaxed by 30 ps molecular dynamics (MD) with all protein and substrate atoms fixed. Stochastic boundary condition [56] was applied to reduce the computational costs. In particular, those atoms outside a 25 Å radius away from the origin were removed, while those in the buffer zone (22 Å < r < 25 Å) were subjected to Langevin dynamics with friction and random forces. In the inner reaction zone (r < 22 Å), the atoms were described by Newtonian dynamics on the hybrid QM/MM potential energy hypersurface. A group-based switching approach was used for nonbonded interactions [57].

Due to a stepwise reaction mechanism for the retaining glycoside hydrolase, it should be noted that the QM regions for the two steps have to be defined differently. Particularly, for the first step of glycosylation, the QM region consists of the xylopentaose, side-chain groups of E127 and E233 residues. Once the glycosylation half reaction is completed, the reduced xylobiose unit will be removed from the active site to facilitate the subsequent deglycosylation step. Meanwhile, a bulk water molecule is introduced to the reaction system for the hydrolysis of the intermediate. The QM region in this step consists of the E233-xylotriose complex, E127 and the water molecule. The covalent interface between QM and MM regions was treated using link atom approach [58].

The QM/MM MD simulations of the enzyme systems were carried out for three different model structures: the enzyme–substrate (ES) complex, enzyme–intermediate (EI) complex with the xylobiose leaving group in the active site, and EI complex without this xylobiose unit. Since our initial ES model was obtained by replacing the crystallized thio-xylopentaose with xylopentaose, an extensive MD relaxation calculation was required. We first performed 500 ps constrained MD simulation to keep the hydrogen bond between E127 and O_4(+1) for the ES complex. The system was first heated slowly from 0 to 300 K within 30 ps, followed by 470 ps MD simulation at room temperature. The resulting system was then subjected to a further 1.4 ns unconstrained MD simulation at room temperature with the final 1.1 ns MD trajectory for data analysis. For the intermediate complex, a 1.1 ns MD simulation was performed with first 300 ps for heating and equilibration, and remaining 800 ps for data analysis. The integration time step for MD was 1 fs, and SHAKE algorithm [59] was applied to keep all covalent bonds involving hydrogen atoms.

To understand the reaction process, we extracted some snapshots from the MD trajectory of the ES complex. After minimization, the potential energy surface was calculated using an adiabatic mapping method (sometimes referred to reaction coordinate driving method; details can be seen in Ref. [60]) along the putative reaction coordinates. For the glycosylation step, the reaction coordinates were defined as $d_1 = d_{C_1(-1)-O_4(+1)} - d_{O_{\varepsilon 1}(E233)-C_1(-1)}$ and $d_2 = d_{O_{\varepsilon 2}(E127)-H_{\varepsilon 2}(E127)} - d_{H_{\varepsilon 2}(E127)-O_4(+1)}$, while $d_3 = d_{C_1(-1)-O_{\varepsilon 1}(E233)} - d_{C_1(-1)-O_W}$ and $d_4 = d_{O_W-H_W} - d_{H_W-O_{\varepsilon 2}(E127)}$ for the deglycosylation step. These calculated configurations along the putative reaction coordinates were used as the initial structures in the two dimensional (2D) potentials of mean force (PMF) calculations. In the PMF calculations, umbrella sampling [61] with harmonic constraints around 100–300 kcal/mol Å^2 were used to enhance sampling. Total of 231 windows were used for both glycosylation and deglycosylation steps, respectively. For each window, 60 ps constrained dynamics simulation was carried out, with the first 30 ps for heating and equilibration, the rest of 30 ps simulation for data analysis. Finally, the weighted histogram analysis method (WHAM) [62,63] was used to obtain the 2D PMF.

To gain mechanistic insights into the reaction process, we further performed the natural bond orbital (NBO) [64] analyses, in which B3LYP/MM//SCC-DFTB/MM single point calculations for all of the stationary points. In this work, the standard basis set of 6-31G(d) was employed. These calculations were performed using the CHARMM interfaced GAMESS-UK package [65].

3. Results and discussion

3.1. Enzyme–substrate complex

A reasonable enzyme–substrate (ES) complex structure is critical for the study of the catalytic mechanism, as well as the rational design of the protein. In this work, a total of 1.9 ns MD simulations were carried out to examine the binding pattern of the

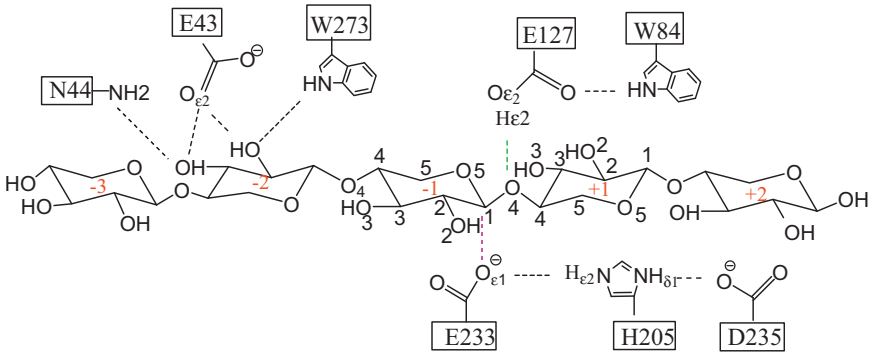

Scheme 2. Atomic interactions between xylopentaose and nearby protein residues. For better view, we plot E127 and E233 residues on different sides of the substrate.

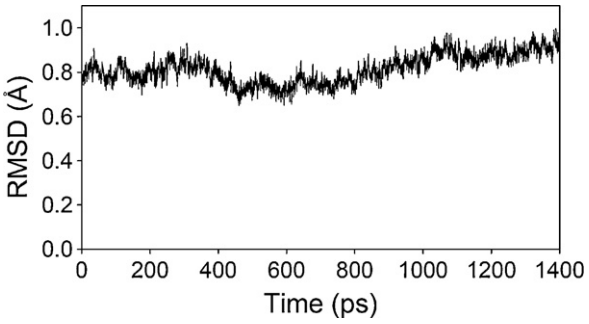

Fig. 1. RMSD for the backbone atoms of the enzyme–substrate complex.

enzyme–xylopentaose complex. It is known that there are two substrate recognition domains in glycoside hydrolases, namely the catalytic domain and the carbohydrate binding module (CBM). Here, we will focus on the binding mode of the xylopentaose with the catalytic domain.

The ES complex is quite stable during the MD simulation, demonstrated by the root mean square deviation (RMSD) for the backbone atoms of 0.82 ± 0.07 Å, as shown by Fig. 1. A snapshot for the ES complex from the MD trajectory is displayed in Fig. 2, and several selected geometric parameters are listed in Table 1. To examine conformational changes in the sugar ring, we have employed Berces' definition of torsion angles [42], in which a general data set of $T = \{\tau_1, \tau_2, \tau_3, \tau_4, \tau_5, \tau_6\}$ is defined as a vector of six endocyclic torsion angles of $C_1C_2C_3C_4$, $C_2C_3C_4C_5$, $C_3C_4C_5O_5$, $C_4C_5O_5C_1$, $C_5O_5C_1C_2$, $O_5C_1C_2C_3$, respectively. In Table 1, we listed six torsion angles for the −1 sugar unit. Interestingly, while has an approximate $^4C_1$ conformation in the X-ray structure, it becomes a somewhat twisted $B_{2,5}$ conformation when a *bona fide* substrate is present in the active site. Such a conformation is quite stable throughout the MD simulation. This indicates that a twisted boat conformer might represent a possible reactive conformation, which is consistent with a recent molecule dynamics simulation [36] for Cex from *C. fimi*, although a $B_{3,O}$ conformation for the sugar unit at the −1 subsite was proposed.

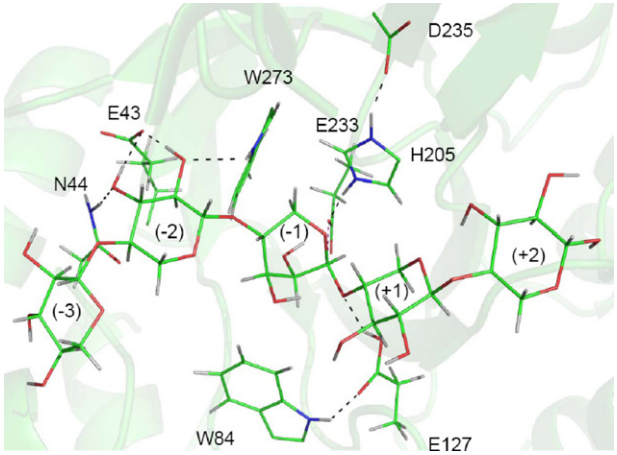

Fig. 2. Snapshot for the enzyme–substrate complex. Black dash lines represent the hydrogen bonds, and purple dash line the nucleophilic attack direction. (For interpretation of the references to color in this figure legend, the reader is referred to the web version of the article.)

One of the special geometric characteristics for a prototypical retaining glycoside hydrolase is that the two conserved carboxylate groups should be placed about 5.5 Å away [8,11]. In our simulations, the distance between two $O_{\varepsilon 2}$ atoms of E127 and E233 is about 5.23 ± 0.31 Å, which is in fairly good agreement with the experimental value of 5.24 Å. The distance between $O_{\varepsilon 1}$ and $C_1(-1)$ is about 3.27 ± 0.23 Å, which suggests the E233 nucleophile is in a perfect near-attack position. This residue is further stabilized by a hydrogen bond provided by H205, judged by the distance of 1.66 ± 0.10 Å between $O_{\varepsilon 1}$(E233) and $H_{\varepsilon 2}$(H205). Interestingly, this positively charged H205 could also form a strong hydrogen bond with D235 to hold its position, evidenced by the $d_{H_{\delta 1}(H205)\ldots O_{\delta 2}(D235)}$ distance of 1.60 ± 0.07 Å. The importance of three conserved residues of E233, H205, and D235 in the GH10 family has been discussed by Notenboom et al. [28].

On the other hand, as the general acid in the glycosylation half reaction, a hydrogen bond with a distance of 2.15 ± 0.37 Å is found between the $O_{\varepsilon 2}$ atom of E127 and the glycosidic oxygen atom $O_4(+1)$ during the simulation. Additionally, E127 is also positioned by a hydrogen bond provided by W84 with a $d_{O_{\varepsilon 1}\ldots H_{\varepsilon 1}(W84)}$ distance of 2.13 ± 0.35 Å. Since the xylopentaose molecule occupies subsites from −3 to +2 of enzyme binding crevice, it would be interesting to examine some specific interactions of the pyranose units with the protein environment. For example, two hydrogen bonds between hydroxyl groups of −2 sugar unit and side chain groups of E43 can be found, evidenced by the $d_{HO_2(-2)\ldots O_{\varepsilon 2}}$ of 1.72 ± 0.16 Å and $d_{HO_3(-2)\ldots O_{\varepsilon 2}}$ of 1.87 ± 0.44 Å.

3.2. Enzyme–intermediate complexes

To confirm Koshland's framework [7] that a typical retaining glycosidase has a stable covalent glycosyl-enzyme intermediate, it is necessary to perform the MD simulation to examine stability of the glycosyl-enzyme intermediate complex. In this work, two 1.1 ns MD simulations were carried out for two different intermediate models with (EI1) and without (EI2) the xylobiose reducing unit in the active site.

The initial structure of EI1 was obtained from the minimum energy path calculation after formation of the glycosyl-enzyme intermediate complex. After minimization of this structure, it was

Table 1
Selected geometric parameters for stationary points for the glycosylation step of the hydrolysis of xylopentaose catalyzed by Cex from *C. fimi* obtained using the SCC-DFTB/MM method. The statistically averaged values from our QM/MM MD simulation for ES and EI1 are also included.*

Distances (Å) angles (°)	Glycosylation step				MD (ES)	MD (EI1)
	Exp. [34]	ES	TS1	EI1		
$C_1(-1)\ldots O_{\varepsilon1}(E233)$	4.04	3.56	2.19	1.50	3.27 ± 0.23	1.48 ± 0.04
$C_1(-1)\ldots O_4(+1)$	1.84[c]	1.50	2.19	3.93	1.50 ± 0.04	6.09 ± 1.00
$C_1(-1)\ldots O_5(-1)$	1.44	1.44	1.31	1.43	1.45 ± 0.03	1.45 ± 0.03
$C_\delta(E127)\ldots C_\delta(E233)$	6.77	6.67	6.39	6.61	6.82 ± 0.26	7.50 ± 0.34
$O_{\varepsilon1}(E233)\ldots H_{\varepsilon2}(H205)$	2.83[b]	1.59	1.73	2.92	1.66 ± 0.10	–
$H_{\delta1}(H205)\ldots O_{\delta2}(D235)$	3.33[b]	1.56	1.56	1.58	1.60 ± 0.07	1.63 ± 0.08
$H_{\varepsilon2}(E127)\ldots O_4(+1)$	3.37[d]	1.88	1.08	1.03	2.15 ± 0.37	1.00 ± 0.02
$H_{\varepsilon2}(E127)\ldots O_{\varepsilon2}(E127)$	–	1.00	1.47	1.66	–	–
$O_{\varepsilon1}(E127)\ldots H_{\varepsilon1}(W84)$	2.85[b]	1.92	1.78	1.77	2.13 ± 0.35	2.00 ± 0.20
$H_{\varepsilon1}(W273)\ldots O_2(-2)$	3.00[b]	2.61	2.45	2.34	2.38 ± 0.29	2.07 ± 0.20
$H_{\delta21}(N44)\ldots O_3(-2)$	2.92[b]	2.03	2.04	2.02	2.15 ± 0.26	2.12 ± 0.23
$O_{\varepsilon2}(E43)\ldots HO_2(-2)$	2.77[a]	1.67	1.65	1.65	1.72 ± 0.17	–
$O_{\varepsilon2}(E43)\ldots HO_3(-2)$	3.50[a]	1.74	1.77	1.77	1.93 ± 0.45	–
$O_{\varepsilon2}(E127)\ldots O_{\varepsilon2}(E233)$	5.24	5.39	4.88	5.00	5.23 ± 0.31	5.64 ± 0.43
τ_1	−51.6	54.7	43.7	31.7	52.4 ± 6.9	53.9 ± 6.1
τ_2	43.7	−9.9	−11.2	−16.8	−8.0 ± 7.9	−29.7 ± 6.9
τ_3	−50.9	−46.7	−37.4	−32.3	−48.4 ± 6.4	−30.2 ± 7.2
τ_4	65.9	61.5	59.3	73.8	64.3 ± 7.7	72.5 ± 6.1
τ_5	−69.1	−14.7	−24.8	−57.7	−18.2 ± 8.8	−46.9 ± 6.7
τ_6	63.1	−42.9	−26.5	5.13	−39.6 ± 6.7	−14.9 ± 6.9
$O_5(-1)\ldots C_1(-1)\ldots C_2(-1)\ldots H_1(-1)$	–	124.8	−171.0	−120.1	124.3 ± 4.8	−120.4 ± 4.8

[a] O—O distance.
[b] O—N distance.
[c] C—S distance.
[d] H—S distance.
* The names of protein atoms are followed CHARMM convention, while those for xylopentaose molecule are named with IUPAC conventions.

subjected to further MD simulations. Throughout the MD simulations, the glycosyl-enzyme intermediate complex is very stable when xylobiose is in the active site of the enzyme. The covalent bond between the $O_{\varepsilon1}(E233)$ atom and substrate anomeric carbon $C_1(-1)$ atom is well maintained with a distance of 1.48 ± 0.04 Å. A snapshot extracted from the trajectory is displayed in Fig. 3. Interestingly, we can observe that the xylobiose molecule has the trend to move out from the active site, judged by the distance between $O_4(+1)$ and $C_1(-1)$ of 6.09 ± 1.00 Å. On the other hand, no stable hydrogen bond can be found between the leaving group and E127. Such a structural change can leave sufficient space to accommodate a water molecule in the active site, which could play the role of nucleophile in the subsequent degylcosylation. Indeed, during the MD simulation, this water molecule can be found in the active site. Interestingly, the distance between C_1 and the oxygen atom of the water molecule is about 3.61 ± 0.46 Å, which indicates that this water is ready for the nucleophilic attack at the C_1 atom to initiate the deglycosylation reaction. A hydrogen bond is formed between this water and E127 side chain group, evidenced by the $d_{H_{w1}\ldots O_{\varepsilon1}(E127)}$ distance of 2.02 ± 0.51 Å. However, the direct attack by water molecule at the anomeric center of $C_1(-1)$ was found to result in a much high barrier. Clearly, the cleavage of the covalent glycosyl-enzyme bond is not possible if the xylobiose molecule is in the active site. Therefore, it would be desired to perform MD simulation of the glcosyl-enzyme intermediate complex after the removal of this xylobiose molecule from the active site.

To carry out the MD simulation of enzyme–intermediate complex without the xylobiose leaving group, we removed the xylobiose molecule from the active site, then the entire system was solvated again, using essentially the same protocol as we have

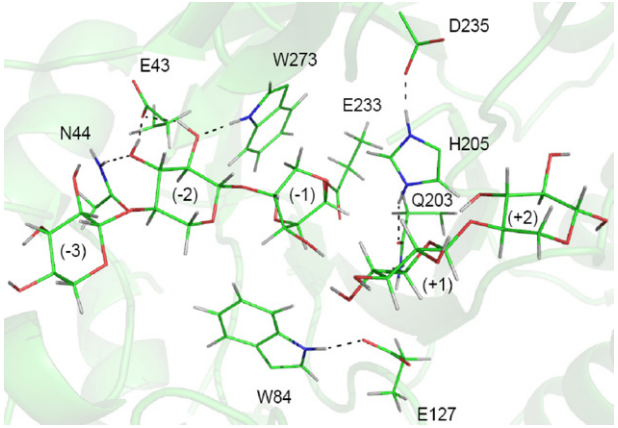

Fig. 3. Snapshot for the glycosyl-enzyme intermediate with the xylobiose molecule in the active site. Black dash lines represent hydrogen bonds.

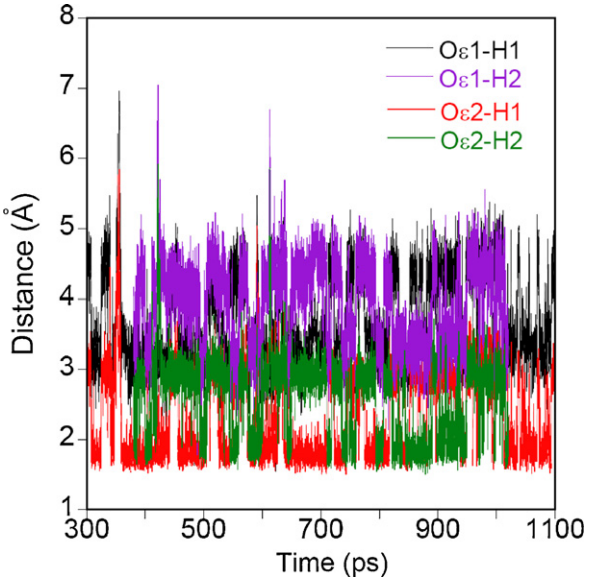

Fig. 4. Distances between hydrogen atoms of water and side chain group of E127 extracted from the trajectory of the MD simulation of the model of EI2.

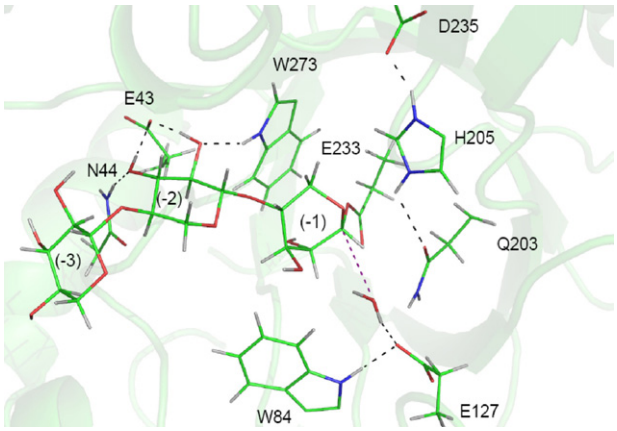

Fig. 5. Snapshot for the glycosyl-enzyme intermediate without the xylobiose molecule in the active site. Black dash lines represent the hydrogen bonds, and purple dash line the nucleophilic attack direction. (For interpretation of the references to color in this figure legend, the reader is referred to the web version of the article.)

addressed in Section 2. One water molecule has been identified in the active site, which forms a hydrogen bond with E127 side chain group. The minimized structure was subjected to further MD simulations to elucidate the role of E127 in the deglycosylation step. To test the possibility of water as the candidate of nucleophile, we did not include water molecule in the QM region. Interestingly, this water can stably stay in the active site. The $d_{O_w \ldots C_1(-1)}$ distance is about 3.88 ± 0.41 Å, which indicates it can serve as the nucleophile to hydrolyze the glycosyl-enzyme intermediate. On the other hand, the hydrogen bond between the water and E127 is well maintained during most of simulation trajectory, as shown in Fig. 4. A snapshot for this glycosyl-enzyme intermediate is depicted in Fig. 5. Clearly, this observation supports the hypothesis that E127 acts as the general base in the deglycosylation reaction. Meanwhile, the covalent glycosyl-enzyme bond between E233 and xylotriose is well kept with the $d_{C_1(-1)\ldots O_{\varepsilon 1}(E233)}$ distance of 1.48 ± 0.04 Å.

3.3. Reaction paths

Calculated reaction potential energy surfaces for the hydrolysis of xylopentaose catalyzed by Cex from *C. fimi* using the hybrid SCC-DFTB/MM method are displayed in Fig. 6. Snapshots for all six stationary points for both glycosylation and deglycosylation steps are given in Fig. 7. For glycosylation, starting from a snapshot extracted from the MD trajectory of the ES complex, we performed a potential energy scan calculation along the putative reaction coordinates (d_1 and d_2) using the adiabatic mapping approach. It might be desired to perform more calculations from different initial states to get more accurate information of energy barriers. However, what we focus in this work is to qualitatively investigate the viability of the retention mechanism. Current simulations are sufficient to support this as discussed below. Clearly, the formation of covalent glycosyl-enzyme and proton transfer from E127 to the atom of $O_4(+1)$ is a completely concerted process. Meanwhile, only one transition state can be located, as shown in Fig. 6A. The corresponding geometric parameters for all three stationary points are listed in Table 1. As the approaching of the nucleophile to the anomeric carbon center of $C_1(-1)$ atom, the distance of β-1,4-xylosidic bond of $C_1(-1)$ and $O_4(+1)$ is elongated from 1.50 Å to 2.19 Å. As the cleavage of C_1—O_4 bond, an alpha glycosyl-enzyme covalent bond is finally formed, with the H_1 atom repelled from its alpha to beta position, judged by the dihedral angle of O_5—C_1—C_2—H_1 changes from 124.8° to −120.1°. Meanwhile, the formation of a partial double bond is evidenced by the bond distance of $C_1(-1)$ and $O_5(-1)$ shortening from 1.44 Å to 1.31 Å.

Table 2
Selected geometric parameters for stationary points along the deglycosylation path of the *C. fimi* Cex catalyzed hydrolysis of xylopentaose calculated using SCC-DFTB/MM method. Geometries from the QM/MM MD simulation of EI2 were also listed in the table for comparison.

Distances (Å) angles (°)	Deglycosylation step			
	MD(EI2)	EI2	TS2	EP
$C_1(-1)\ldots O_{\varepsilon 1}(E233)$	1.48 ± 0.04	1.49	2.28	2.99
$O_w \ldots C_1(-1)$	3.88 ± 0.41	3.30	2.08	1.46
$C_1(-1)\ldots O_5(-1)$	1.45 ± 0.04	1.44	1.33	1.47
$H_w \ldots O_{\varepsilon 2}(E127)$	–	1.69	1.13	1.00
$H_w \ldots O_w$	–	1.01	1.33	1.81
$O_{\varepsilon 2}(E43)\ldots HO_2(-2)$	1.71 ± 0.15	1.62	1.63	1.64
$O_{\varepsilon 2}(E43)\ldots HO_3(-2)$	1.80 ± 0.35	1.73	1.70	1.69
$O_{\varepsilon 2}(E127)\ldots H_{\varepsilon 1}(W84)$	2.02 ± 0.19	1.79	1.81	1.88
$H_{\delta 1}(H205)\ldots O_{\delta 2}(D235)$	1.63 ± 0.10	1.60	1.57	1.57
$O_{\varepsilon 1}(E233)\ldots H_{\varepsilon 2}(H205)$	–	2.88	1.69	1.61
$H_{\varepsilon 2}(H205)\ldots O_{\varepsilon 1}(Q203)$	1.86 ± 0.19	1.81	2.89	3.09
$H_{\varepsilon 1}(W273)\ldots O_2(-2)$	2.07 ± 0.18	2.14	2.24	2.47
$H_{\delta 21}(N44)\ldots O_3(-2)$	2.19 ± 0.25	1.87	1.87	1.87
τ_1	55.2 ± 6.1	49.4	51.1	59.9
τ_2	−31.7 ± 6.5	−29.6	−17.7	−22.5
τ_3	−29.3 ± 6.8	−28.3	−35.4	−40.0
τ_4	73.3 ± 5.8	73.8	61.8	71.4
τ_5	−48.3 ± 6.8	−52.9	−26.8	−32.6
τ_6	−14.3 ± 7.3	−7.58	−29.1	−31.3
$O_5(-1)$—$C_1(-1)$—$C_2(-1)$—$H_1(-1)$	−120.1 ± 4.8	−120.8	171.8	123.9

The hybridization bond nature around O_5 atom along the reaction path deserves some discussion. Based on our NBO analyses using B3LYP/MM//SCC-DFTB/MM single point calculations, the C_1—O_5 bond is almost pure sp^3 hybridization before glycosylation: $\psi^{NBO}_{O_5-C_1} = 0.573\sigma_{sp^{3.65}(C_1)} + 0.819\sigma_{sp^{2.74}(O_5)}$, while the glycosylation transforms O_5 to predominantly sp^2 hybridization in the transition state: $\psi^{NBO}_{O_5-C_1} = 0.558\sigma_{sp^{2.83}(C_1)} + 0.830\sigma_{sp^{1.77}(O_5)}$. Meanwhile, the charge on O_5 becomes more positive (−0.58 in ES vs. −0.49 in TS1). On the other hand, a near planar O_5—C_1—C_2—H_1 (−171.0°) can be found at the transition state. In addition, based on the values of {τ_1, τ_2, τ_3, τ_4, τ_5, τ_6}, the transition state cannot be classified as the $^3H_4$ or $^4H_3$ conformation. However, a mixed conformer of $B_{2,5}$ and $^OS_2$ is more likely[42]. All evidences clearly indicate the formation of an oxo-carbenium ion-like transition state. With the generation of the covalent intermediate, the proton was fully transferred to $O_4(+1)$ atom to produce the xylobiose molecule and an ionized E127 residue. Clearly, the E127 residue should serve as the acid catalyst during the glycosylation step. At the same time, the ionization of E127 makes it a candidate for the general base in the subsequent deglycosylation reaction.

As pointed by our MD simulation of the glycosyl-enzyme intermediate, the xylobiose molecule has to be removed from the active site to facilitate the cleavage of the covalent glycosyl-enzyme bond. The water molecule, which is hydrogen bonded with E127, is further postulated to act as the nucleophile, while E127 plays the role of general base. Indeed, only one transition state for the cleavage of covalent glycosyl-enzyme bond can be located from the potential energy surface calculations at the SCC-DFTB/MM level of theory, as shown in Fig. 6B. Selected geometric properties of three stationary points for deglycosylation are reported in Table 2. The nucleophilic attack to anomeric carbon $C_1(-1)$ is initiated by the proton transfer from water to E127. With the cleavage of glycosyl-enzyme covalent bond, the conformation around the anomeric center of $C_1(-1)$ recovers its original β conformation, which is the basic characteristic of net retention mechanism. Further analysis of conformations for three stationary points at this part of reaction also indicates that it has a significant conformational change as that in glycosylation step. Interestingly, with the release of the xylobiose molecule, the conformation of the sugar ring changes from $^OS_2$ to a mixed $^OS_2/^{3,O}B$ at the transition state, based on the torsion angles shown in Table 2.

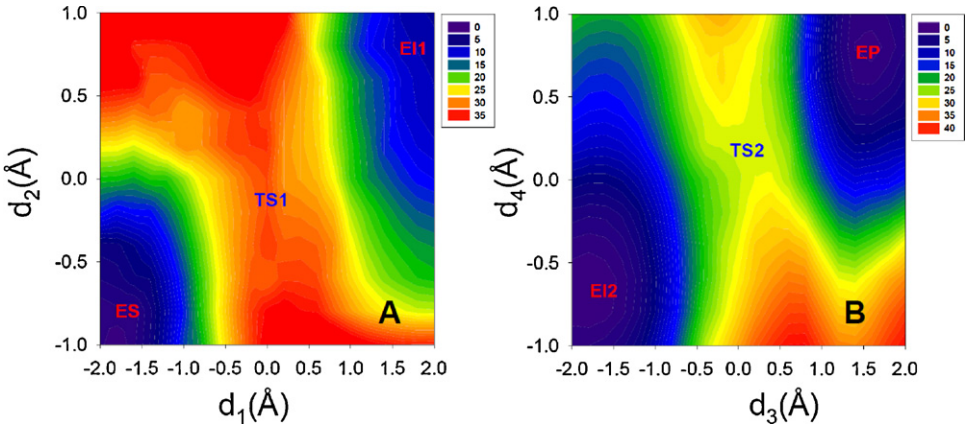

Fig. 6. Potential energy surfaces for both glycosylation (A) and deglycosylation (B) steps using the SCC-DFTB/MM method. Contours are separated by 1 kcal/mol.

The shape of the sugar at −1 site finally changes to an approximate skew boat, $^{O}S_2$, although τ_4 of 71.4° is a bit larger than ideal value of 60°. Finally, the detailed reaction mechanisms are summarized in Scheme 3.

3.4. Potentials of mean force

Although minimum energy path calculations can shed some lights on the catalytic mechanism by Cex from *C. fimi*, entropy effects were not included. To account for dynamic effects caused by the enzyme and bulk solvent environment, we further carried out free energy simulations for two steps of reactions along putative reaction coordinates, respectively.

The calculated free energy surfaces are depicted in Fig. 8. Consistent with our reaction path calculations, only one transition state can be located for both glycosylation and deglycosylation reactions. The calculated free energy barrier is about 24.3 kcal/mol for the formation of glycosyl-enzyme intermediate, whereas it needs about

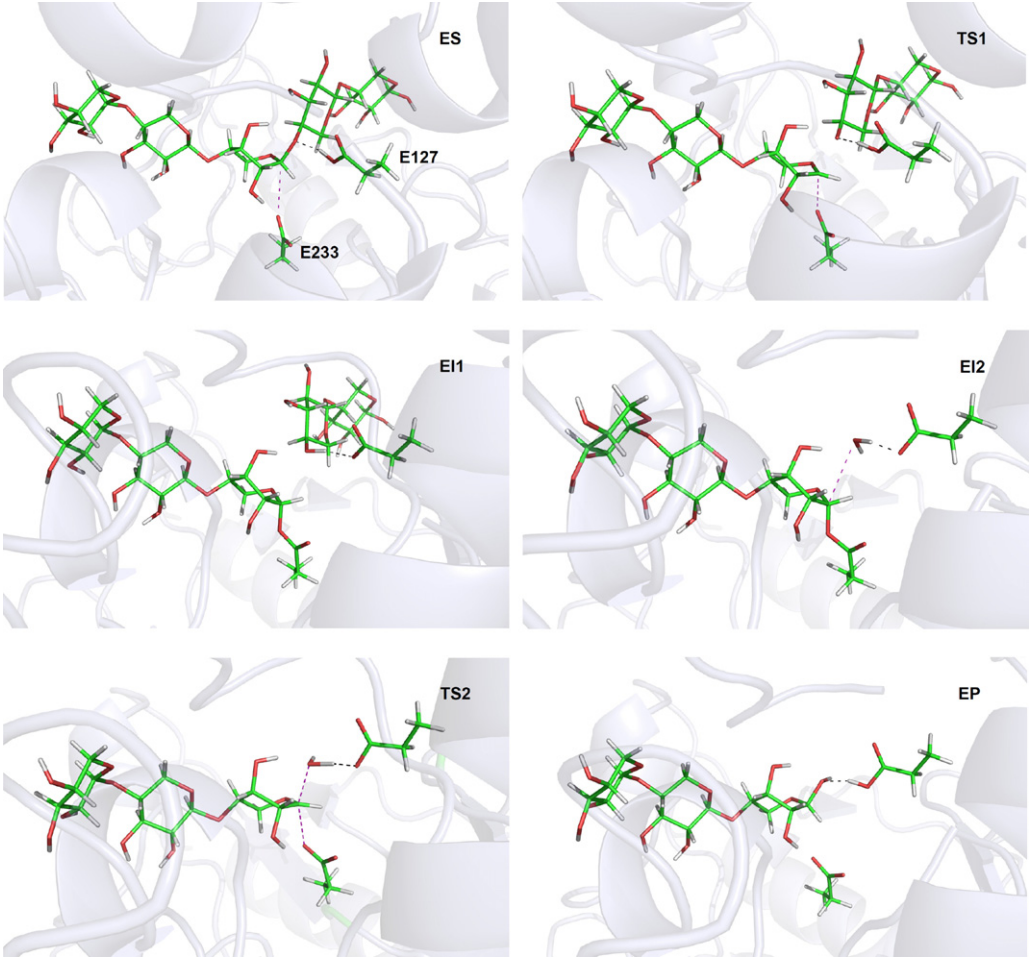

Fig. 7. Snapshots of QM/MM stationary states along the reaction path for Cex catalyzed hydrolysis of xylopentaose. ES, TS1 and EI1 are for glycosylation half reaction, while EI2, TS2 and EP are for deglycosylation half reaction.

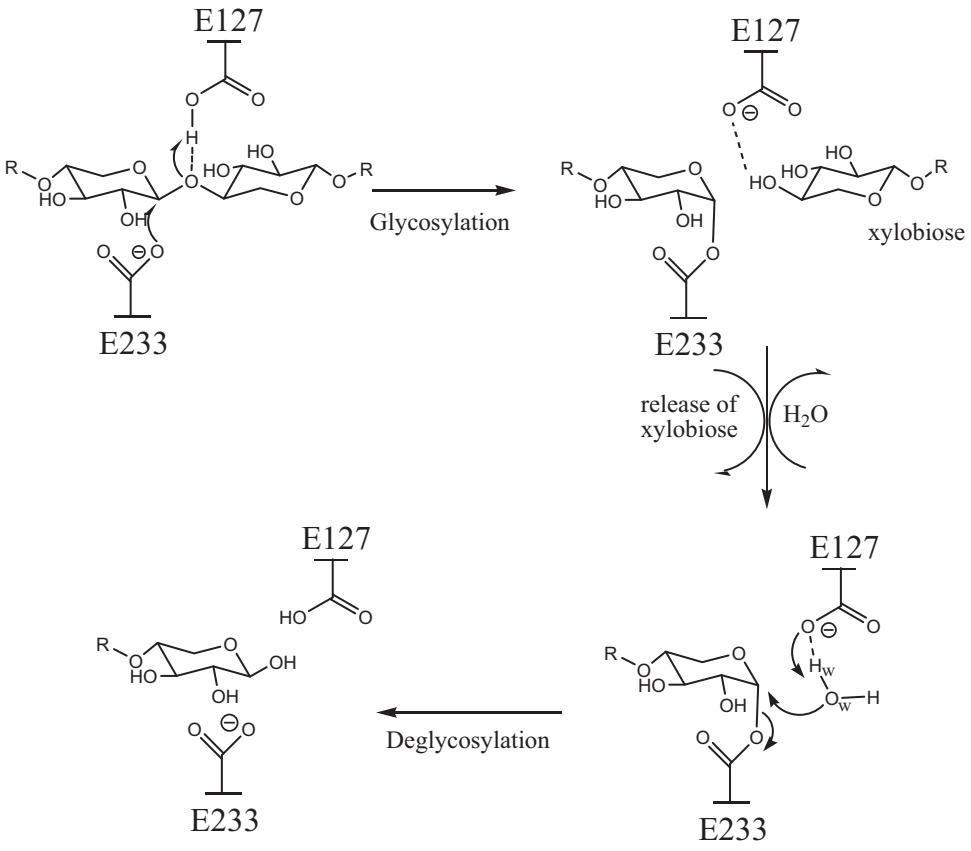

Scheme 3. Proposed catalytic mechanism for the hydrolysis of xylopentaose catalyzed by Xylanase Cex from *C. fimi*.

35.0 kcal/mol for the hydrolysis of the covalent intermediate. The energy barriers were reported using the energy difference between TS1 and ES for glycosylation, and difference between TS2 and EI2 for deglycosylation, respectively. Unfortunately, no direct kinetic data for the hydrolysis of xylopentaose catalyzed by Cex from *C. fimi* have been reported so far. Hence, the direct comparison with experimental data is not possible. The second barrier seems to be relatively high, which might be due to the semi-empirical method we used in our simulations. Clearly, only qualitative description of the overall energy barrier can be expected in this work. A higher level QM approach, such as an ab initio method, combined with molecular mechanical method might be more suitable to calculate the free energy profile for the system like glycosidases. On the other hand, due to the removal of the xylobiose molecule, extensive reorganization of protein is required to reach sufficient relaxation to perform the next reaction. This might be another reason that generates the high second barrier. Nevertheless, we need to emphasize here that the retaining mechanism can be well established for Cex from *C. fimi*.

3.5. Site-directed mutagenesis molecular dynamics simulations

Another interesting issue is the sugar ring distortion during the substrate binding. It has long been accepted that the ring conformation plays an important role in the function and reactivity of carbohydrates [42,66]. It is quite common that the sugar ring at −1 site cannot keep the ideal chair ($^1C_4$ or $^4C_1$) conformation when substrate binding in the active site. In the current

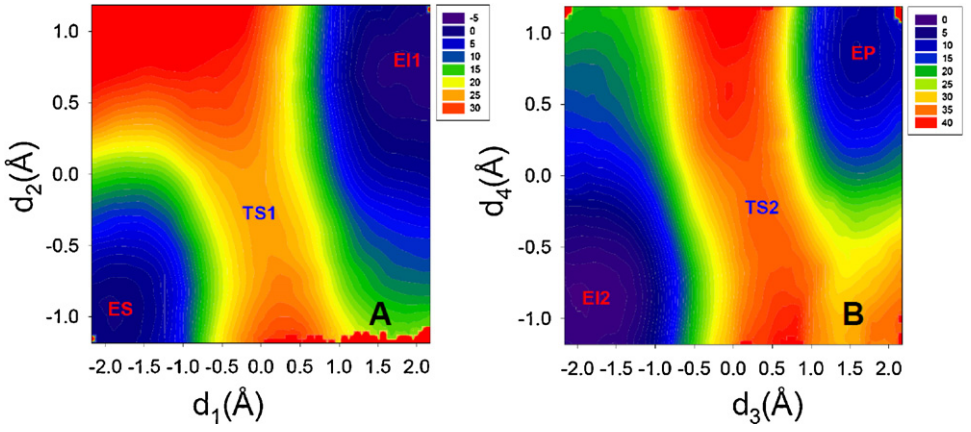

Fig. 8. Calculated potentials of mean force for both glycosylation (A) and deglycosylation (B) processes. Contours are separated by 1 kcal/mol.

Table 3
The statistically averaged endocyclic torsion angles for the ES complex of the wide type and mutants.

Torsion angles (°)	X-ray [34]	E127A	E233A	E127A/E233A	WT
τ_1	−51.6	−47.6 ± 8.9	−41.9 ± 8.9	−48.7 ± 7.8	52.4 ± 6.9
τ_2	43.7	45.7 ± 7.4	37.7 ± 8.6	47.2 ± 7.1	−8.0 ± 7.9
τ_3	−50.9	−53.1 ± 6.7	−47.2 ± 7.5	−54.1 ± 6.1	−48.4 ± 6.4
τ_4	65.9	62.8 ± 6.9	62.3 ± 6.8	63.7 ± 6.3	64.3 ± 7.7
τ_5	−69.1	−64.4 ± 6.0	−67.0 ± 5.8	−65.3 ± 5.7	−18.2 ± 8.8
τ_6	63.1	56.8 ± 7.4	56.3 ± 6.9	57.4 ± 6.3	−39.6 ± 6.7

system we studied, such distortion has been observed by a classical MD simulation [36], in which the xylotetraose molecule was modeled in the active site of Cex. It was suggested that the substrate at −1 site adopts a $B_{3,O}$ conformation. Furthermore, they proposed that this boat conformation could represent a reactive conformer. In this work, a similar substrate distortion was also observed. However, we found that during the MD simulation the xylose unit at the −1 site distorts to a conformation close to $B_{2,5}$, with rest of four sugar units keep the approximate chair conformation. Considering the initial structure in our simulation is adopted from the X-ray structure, we believe that our model might represent a more probable reactive conformer. More interestingly, as pointed by Deslongchamps [67] "α-glycosides must hydrolyze via their ground state conformation whereas β-glycosides must first assume a boat conformation in order to fulfill the stereo-electronic requirement". The distortion to $B_{2,5}$ conformation in our simulation clearly fulfills the stereo-electronic requirement for hydrolysis.

To identify the specific factor that causes this kind of distortion, more investigations are highly desired. We carried out several MD simulations on mutants of E233A, E127A and E233A/E127A bound with the xylopentaose molecule to test their effects on the conformational change. The protocol of MD simulation is the same as we did for the ES complex. A total of 1 ns MD simulation was carried out for each mutated system. In Table 3, six endocyclic torsion angles (using the same definition as we mentioned above) for the xylose unit at −1 site were listed to show the conformational change. The torsion angles of the mutants are in fairly good agreement with those of X-ray structure, in which the thio-substituted xylopentaose was crystallized in the active site. Typical difference is less than 5° except τ_1 and τ_2 in the mutant of E233A. In addition, the structure of the double mutant is the closest one to the X-ray structure. This might suggest that both catalytic residues (E127 and E233) should contribute to the substrate distortion equally. In other words, this could also be considered as a typical example of enzyme induced substrate reorganization. On the other hand, with the mutation of E127A, the distance between $C_1(-1)$ and $O_{\varepsilon 1}$ (E233) was elongated to 4.91 ± 0.41 Å, which is much longer than 3.27 ± 0.23 Å in wild type.

We have also examined the energy barrier height of the formation of glycosyl-enzyme intermediate for E127A, which is much higher than that for the wild type. Lack of the general acid is of course one of the reasons to cause this, but the deviation from the possible reactive conformer of $B_{2,5}$ cannot be ignored either. Especially for wild type enzyme, the pyranose ring at the −1 subsite takes a boat shape of $B_{2,5}$. Structural characteristics of such conformation can satisfy the requirement for possible reaction. To this point, the ring distortion can no doubt facilitate the first step of formation of covalent glycosyl-enzyme bond. It should be noted that current mutagenesis simulations just considered the effects of two catalyst residues, E127 and E233. It would be interesting to perform some further studies to check if other factors could control this type of process.

4. Conclusions

In this work, we have addressed the detailed hydrolysis mechanism of the xylopentaose molecule catalyzed by Cex from *C. fimi* by means of combined SCC-DFTB/CHARMM approaches. Due to the geometrical characteristics of the active site, we did not pursue the possibility of inversion mechanism for this enzyme. On the other hand, although the calculated free energy barrier height seems a little bit high, our simulations can still support that the hydrolysis reaction via a net retention is reasonable with E233 as the nucleophile and E127 as the acid/base catalyst. The generation of the oxo-carbenium ion transition state was confirmed by the NBO and geometrical analysis. It was shown by QM/MM MD simulations that the xylose unit at the −1 binding site takes the $B_{2,5}$ conformation for the substrate binding. Further mutagenesis studies suggested that two catalytic residues (E127 and E233) play the vital role in the ring distortion. Structural analysis indicates it can facilitate the first step of glycosylation. To fully understand the ring distortion during whole reaction process, it would be better to perform extensive mutant studies, especially including rest of residues around active site.

Acknowledgments

This work was funded by Natural Science Foundation of China (nos. 21073125 and 31170675), and by the Program for New Century Excellent Talents in University (no. NCET-10-0606). Special thanks to Prof. Qiang Cui and Mr. Guanhua Hou (University of Wisconsin, Madison) for technical help in the NBO analysis.

Appendix A. Supplementary data

Supplementary data associated with this article can be found, in the online version, at http://dx.doi.org/10.1016/j.jmgm.2012.04.005.

References

[1] D.I.C. Wang, G.C. Avgerinos, I. Biocic, S.-D. Wang, H.-Y. Fang, Philosophical Transactions of the Royal Society of London B 300 (1983) 323.
[2] L.R. Lynd, J.H. Cushman, R.J. Nichols, C.E. Wyman, Science 251 (1991) 1318.
[3] M. Galbe, G. Zacchi, Applied Biochemistry and Biotechnology 59 (2002) 618.
[4] T. Collins, C. Gerday, G. Feller, FEMS Microbiology Letters 29 (2005) 3.
[5] Q. Wang, T. Xia, World Journal of Microbiology and Biotechnology 23 (2007) 1047.
[6] B. Henrissat, A. Bairoch, Biochemical Journal 316 (1996) 695.
[7] D.E.J. Koshland, Biological Reviews 28 (1953) 416.
[8] D.L. Zechel, S.G. Withers, Accounts of Chemical Research 333 (2000) 11.
[9] D.L. Zechel, S.G. Withers, Current Opinion in Chemical Biology 5 (2001) 643.
[10] A. Vasella, G.J. Davies, M. Bohm, Current Opinion in Chemical Biology 6 (2002) 619.
[11] D.J. Vocadlo, G.J. Davies, Current Opinion in Chemical Biology 12 (2008) 539.
[12] B. Henrissat, G. Davies, Current Opinion in Structural Biology 7 (1997) 637.
[13] K. Li, P. Azadi, R. Collins, J. Tolan, J.S. Kim, K.E.L. Eriksson, Enzyme and Microbial Technology 27 (2000) 89.
[14] A. White, S.G. Withers, N.R. Gilkes, D.R. Rose, Biochemistry 33 (1994) 12546.
[15] W.W. Wakarchuk, R.L. Campbell, W.L. Sung, J. Davoodi, M. Yaguchi, Protein Science 3 (1994) 467.
[16] W.W. Wakarchuk, W.L. Sung, R.L. Campbell, A. Cunningham, D.C. Watson, M. Yaguchi, Protein Science 7 (1994) 1379.

[17] T.M. Gloster, S.J. Williams, S. Roberts, C.A. Tarling, J. Wichki, S.G. Withers, G. Davies, Journal of Chemical Communications (2004) 1794.
[18] A. Schmidt, G.M. Gübitz, C. Kratky, Biochemistry 38 (1999) 2403.
[19] R. Natesh, P. Bhanumoorthy, P.J. Vithayathil, K. Sekar, S. Ramakumar, M.A. Viswamitra, Journal of Molecular Biology 288 (1999) 999.
[20] U. Derewenda, L. Swenson, R. Green, Y. Wei, R. Morosolis, F. Shareck, D. Kluepfel, Z.S. Derewenda, Journal of Biological Chemistry 269 (1994) 20811.
[21] Ihsanawati, T. Kumasaka, T. Kaneko, C. Morokuma, S. Nakamura, N. Tanaka, Acta Crystallographica D59 (2003) 1659.
[22] G. Sihu, S.G. Withers, N.T. Nguyen, L.P. McIntosh, L. Ziser, G.D. Brayer, Biochemistry 38 (1999) 5346.
[23] S. Bedarkar, N.R. Gilkes, D.G. Kilburn, E. Kwan, D.R. Rose, R.C. Miller Jr., R.A. Warren, S.G. Withers, Journal of Molecular Biology 228 (1992) 693.
[24] D. Tull, S.G. Withers, Biochemistry 33 (1994) 6363.
[25] A.M. MacLeod, D. Tull, K. Rupitz, R.A.J. Warren, S.G. Withers, Biochemistry 35 (1996) 13165.
[26] P.V. Nikolova, A.L. Creagh, S.J.B. Duff, C.A. Haynes, Biochemistry 36 (1997) 1381.
[27] V. Notenboom, C. Birsan, R.A.J. Warren, S.G. Withers, D.R. Rose, Biochemistry 37 (1998) 4751.
[28] V. Notenboom, C. Birsan, M. Nitz, D.R. Rose, R.A.J. Warren, S.G. Withers, Nature Structural Biology 5 (1998) 812.
[29] V. Notenboom, S.J. Williams, R. Hoos, S.G. Withers, D.R. Rose, Biochemistry 39 (2000) 11553.
[30] N.R. Gilkes, M. Claeyssens, R. Aebersold, B. Henrissat, A. Meinke, H. Morrison, d.D.G. Kilburn, R.A.J. Warren Jr., R.C. Miller, European Journal of Biochemistry 202 (1991) 367.
[31] B.C. Saha, Journal of Industrial Microbiology and Biotechnology 30 (2003) 279.
[32] S.J. Charnock, T.D. Spurway, H. Xie, M.-H. Beylot, R. Virden, R.A.J. Warren, G.P. Hazlewood, H.J. Gilbert, Journal of Biological Chemistry 273 (1998) 32187.
[33] A. White, D. Tull, K. Johns, S.G. Withers, D.R. Rose, Nature Structural & Molecular Biology 3 (1996) 149.
[34] D.K.Y. Poon, I.D. D'Angelo, D.A. Kuntz, T. Kantner, M.L. Ludiwzek, C. Tarling, D.R. Rose, M. Saul, L.P. McIntosh, S.G. Withers, Probing the binding sites of family 10 and 11 xylanases with extended oligosaccharides (2008).
[35] G. Davies, K. Wilson, B. Henrissat, Biochemical Journal 321 (1997) 557.
[36] M. Kankainen, T. Laitinen, M. Perakyla, Physical Chemistry Chemical Physics 6 (2004) 5074.
[37] M.E.S. Soliman, J.J.R. Pernia, I.R. Greig, I.H. Williams, Organic & Biomolecular Chemistry 7 (2009) 5236.
[38] M.E.S. Soliman, G.D. Ruggiero, J.J.R. Pernia, I.R. Greig, I.H. Williams, Organic & Biomolecular Chemistry 7 (2009) 460.
[39] X. Biarnes, J. Nieto, A. Planas, C. Rovira, Journal of Biological Chemistry 281 (2006) 1432.
[40] X. Biarnes, A. Ardevol, A. Planas, C. Rovirat, A. Laio, M. Parrinello, Journal of the American Chemical Society 129 (2007) 10686.
[41] V.A. Money, N.L. Smith, A. Scffidi, R.V. Stick, H.J. Gilbert, G. Davies, Angewandte Chemie – International Edition 45 (2006) 5136.
[42] A. Berces, D.M. Whitfield, T. Nukada, Tetrahedron 57 (2001) 477.
[43] A. Warshel, M. Levitt, Journal of Molecular Biology 103 (1976) 227.
[44] J. Gao, Accounts of Chemical Research 29 (1996) 298.
[45] J. Gao, S. Ma, D.T. Major, K. Nam, J. Pu, D. Truhlar, Chemical Reviews 106 (2006) 3188.
[46] H. Hu, W.T. Yang, Annual Review of Physical Chemistry 59 (2008) 573.
[47] H.M. Senn, W. Thiel, Angewandte Chemie – International Edition 48 (2009) 1198.
[48] M. Elstner, D. Porezag, G. Jungnickel, J. Elsner, M. Haugk, T. Frauenheim, S. Suhai, G. Seigert, Physical Review B58 (1998) 7260.
[49] Q. Cui, M. Elstner, E. Kaxiras, T. Frauenheim, M. Karplus, Journal of Physical Chemistry B 105 (2001) 569.
[50] D. Xu, H. Guo, Journal of the American Chemical Society 131 (2009) 9780.
[51] D. Xu, H. Guo, Q. Cui, Journal of the American Chemical Society 129 (2007) 10814.
[52] D. Xu, D. Xie, H. Guo, Journal of Biological Chemistry 281 (2006) 8740.
[53] J. Liu, X. Wang, D. Xu, Journal of Physical Chemistry B 114 (2010) 1462.
[54] A.D. MacKerell Jr., D. Bashford, M. Bellott, R.L. Dunbrack Jr., J.D. Evanseck, M.J. Field, S. Fischer, J. Gao, H. Guo, S. Ha, D. Joseph-McCarthy, L. Kuchnir, K. Kuczera, F.T.K. Lau, C. Mattos, S. Michnick, T. Ngo, D.T. Nguyen, B. Prodhom, W.E. Reiher III, B. Roux, M. Schlenkrich, J.C. Smith, R. Stote, J. Straub, M. Watanabe, J. Wiorkiewicz-Kuczera, D. Yin, M. Karplus, Journal of Physical Chemistry B102 (1998) 3586.
[55] W.L. Jorgensen, J. Chandrasekhar, J.D. Madura, R.W. Impey, M.L. Klein, Journal of Chemical Physics 79 (1983) 926.
[56] C.L. Brooks III, A. Brunger, M. Karplus, Biopolymers 24 (1985) 843.
[57] P.J. Steinbach, B.R. Brooks, Journal of Computational Chemistry 15 (1994) 667.
[58] M.J. Field, P.A. Bash, M. Karplus, Journal of Computational Chemistry 11 (1990) 700.
[59] J.-P. Ryckaert, G. Ciccotti, H.J.C. Berendsen, Journal of Computational Physics 23 (1977) 327.
[60] H.L. Woodcock, M. Hodoscek, B.R. Brooks, Journal of Physical Chemistry A 111 (2007) 5720.
[61] G.M. Torrie, J.P. Valleau, Journal of Computational Physics 23 (1977) 187.
[62] S. Kumar, D. Bouzida, R.H. Swendsen, P.A. Kollman, J.M. Rosenberg, Journal of Computational Chemistry 13 (1992) 1011.
[63] B. Roux, Computer Physics Communications 91 (1995) 275.
[64] A.E. Reed, F. Weinhold, Journal of Chemical Physics 78 (1983) 4066.
[65] M.F. Guest, I.J. Bush, H.J.J. van Dam, P. Sherwood, J.M.H. Thomas, J.H. van Lenthe, R.W.A. Havenith, J. Kendrick, Journal of Molecular Physics 103 (2005) 719.
[66] A.J. Kirby, The Anomeric Effect and Related Stereoelectronic Effects at Oxygen, Springer, Heidelberg, 1983.
[67] P. Deslongchamps, Stereoelectronic Effects in Organic Chemistry, Pergamon Press, Oxford, 1983.